Available online at www.sciencedirect.com
SciVerse ScienceDirect
Physics Procedia 45 (2013) 189 – 192
Physics Procedia

ISS2012

$BaFe_2As_2$/Fe bilayers with [001]-tilt grain boundary on MgO and $SrTiO_3$ bicrystal substrates

K. Iida[a*], S. Haindl[b], F. Kurth[a], J. Hänisch[a], L. Schulz[a], B. Holzapfel[a]

[a]*Institute for Metallic Materials, IFW Dresden. 01171 Dresden, Germany*
[b]*Institute for Solid State Research, IFW Dresden. 01171 Dresden, Germany*

Abstract

Co-doped $BaFe_2As_2$ (Ba-122) can be realized on both MgO and $SrTiO_3$ bicrystal substrates with [001]-tilt grain boundary by employing Fe buffer layers. However, an additional spinel (i.e. $MgAl_2O_4$) buffer between Fe and $SrTiO_3$ is necessary since an epitaxial, smooth surface of Fe layer can not be grown on bare $SrTiO_3$. Both types of bicrystal films show good crystalline quality.

Keywords: Pnictide; Grain boundary; Thin film; Bicrystal; Buffer layer

1. Introduction

In high-T_c cuprates, [001]-tilt grain boundaries (GBs) in MgO and $SrTiO_3$ bicrystal substrates have been commonly used for realizing Josephson junctions as well as investigating transport properties of GBs. After the discovery of Fe-based pnictide superconductors,[1] the community became immediately interested in exploring grain boundaries in this new class of superconductors.

Despite the recent success of realizing Co-doped $BaFe_2As_2$ (Ba-122) on [001]-tilt GB MgO and $SrTiO_3$ bicrystal substrates,[2-3] these substrates may not be suitable for several reasons. Firstly, a large misfit between Ba-122 and MgO of around 6 % leads to low crystalline quality or even non-epitaxial growth under our deposition condition.[4] Secondly, the $SrTiO_3$ substrate becomes electrically conductive under ultra-high vacuum (UHV) conditions, which may compromise transport measurements particularly near the normal-superconducting transition. However, implementation of Fe for MgO and Fe+$MgAl_2O_4$ for $SrTiO_3$ as buffer layers can solve those problems. An Fe layer itself is electrically conductive, however, the recalculation of the superconducting transition temperature (T_c) and the critical current density (J_c) is possible due to its thin layer thickness (20 nm).[5] In this report, the fabrication of Co-doped Ba-122 thin films on both [001]-tilt bicrystal MgO and $SrTiO_3$ substrates and their transport properties are presented in detail. For the aim of bicrystal Josephson junctions, substrates with a large [001]-tilt angle of over 20° have been used in this investigation.

2. Experimental procedure

* Corresponding author. Tel.:+49-351-4659-608; fax: +49-351-4659-541.
E-mail address: k.iida@ifw-dresden.de

doi:10.1016/j.phpro.2013.04.084

2.1. Ba-122 on [001]-tilt MgO bicrystal

A 20 nm thick Fe buffer layer was deposited by means of pulse laser deposition (PLD) on a [001]-tilt MgO bicrystal substrate with misorientation angle of θ_{GB}=36.8° (nominal value) at room temperature, followed by a high-temperature annealing at 700°C. This process is very effective for obtaining epitaxial Fe layers with flat surface. After the Fe buffer preparation, Co-doped Ba-122 ($BaFe_{1.8}Co_{0.2}As_2$) with 100 nm thickness was deposited at 700 °C. All deposition processes have been conducted under UHV condition. A detailed description of both Fe buffer and Co-doped Ba-122 deposition procedure can be found in Ref. [6]. After the structural characterization described in sub-section *2.3*, Au layers were deposited on the films by PLD at room temperature followed by ion beam etching to fabricate bridges of 0.5 mm width and 1 mm length for transport measurements.

2.2. Ba-122 on [001]-tilt $SrTiO_3$ bicrystal

A $MgAl_2O_4$ buffer was deposited on a [001]-tilt GB $SrTiO_3$ bicrystal substrate with θ_{GB} = 30° at 650 °C by PLD in UHV condition (pulse number 4000 at 40 mJ). In a pilot experiment, we have confirmed that $MgAl_2O_4$ can be grown epitaxially on $SrTiO_3$ (100) substrate. After the primary buffer deposition, the $MgAl_2O_4$-buffered $SrTiO_3$ substrate was cooled to room temperature for the secondary, Fe buffer deposition. A 20 nm thick Fe buffer was prepared by the same procedure as described in sub-section *2.1* except for the annealing temperature. Here, a slightly higher temperature of 750°C was employed. After the Fe buffer preparation, a 100 nm thick Co-doped Ba-122 ($BaFe_{1.84}Co_{0.16}As_2$) layer was deposited. *In-situ* gold layer deposition at room temperature was conducted after the Ba-122 deposition for the aim of protection from possible damage during the structuring process.

2.3. Structural characterization and transport measurements

Phase purity and out-of-plane texture were investigated by means of X-ray diffraction in Bragg-Brentano geometry with Co-K$_\alpha$ radiation. In-plane orientation of both Fe and Co-doped Ba-122 were investigated by using the 110 and 103 poles, respectively, in a texture goniometer operating with Cu-K$_\alpha$ radiation. The respective measured reflection of the MgO and $SrTiO_3$ bicrystal substrates for in-plane texture measurements are 220 and 110.

Superconducting properties were measured in a Physical Property Measurement System (PPMS, Quantum Design) by a standard four-probe method with a criterion of 1 μVcm^{-1} for evaluating J_c.

3. Results and discussion

XRD patterns in logarithmic scale (fig. 1 (a)) clearly show that the film has been grown with high phase purity and *c*-axis texture, i.e. with [001] perpendicular to the substrate surface. Fig. 1 (b) shows the ϕ-scans of the 103 Ba-122, the 110 Fe and the 220 MgO. It is evident from fig. 1 (b) that two grains with θ_{GB}~37.1°, which is slightly larger than the nominal value of 36.8°, are grown due to the perfect transfer of the grain orientation from the substrate via Fe buffer to the Ba-122 layer. Here the respective average $\Delta\phi_{Ba\text{-}122}$ and $\Delta\phi_{Fe}$ are 0.84° and 0.80° (not corrected for instrumental broadening), indicative of good in-plane alignment for both layers. The GB is symmetric, i.e. it is situated with $\theta_{GB}/2$ to (100) in both grains.

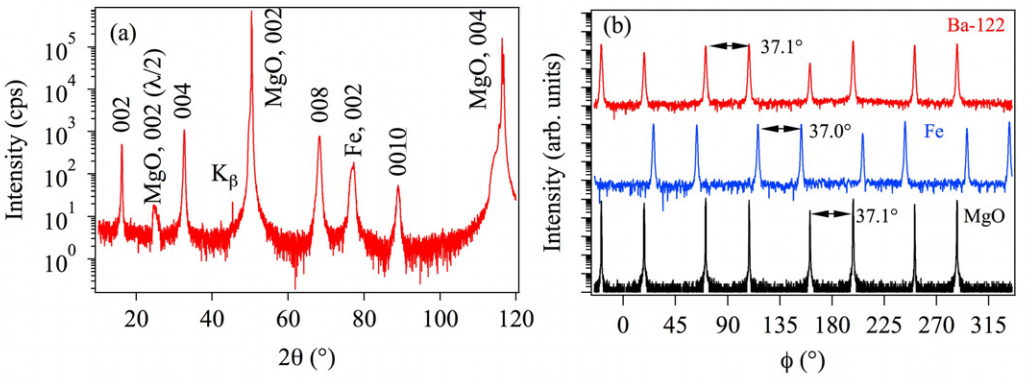

Fig. 1. (a) The θ/2θ scan of Ba-122/Fe bilayer on [001]-tilt GB MgO bicrystal substrate in Bragg- Brentano geometry using Co-Kα radiation. (b) The ϕ-scans of the 103 Ba-122, the 110 Fe and the 220 MgO. Average misorientation angles are 37.1°, 37.0°, and 37.1° for Ba-122, Fe and MgO, respectively.

R-T curves in fig. 2 (a) show that both the inter- and intra-grain bridge have the same onset T_c as well as zero resistance, indicating the high quality of the bicrystal films. The field dependence of $J_c(B||c)$ for both the inter- and intra-grain bridge at various temperatures is displayed in fig. 2 (b). Clearly, the intra-grain J_c (J_c^{intra}) is higher than the inter-grain J_c (J_c^{inter}) at low magnetic fields regime due to the large θ_{GB}. The difference between J_c^{intra} and J_c^{inter} is getting smaller with increasing applied field and finally both curves overlap at the irreversibility field for $\theta_{GB} \sim 37°$. On the assumption that the weak-link behavior is empirically described by $J_c^{inter}=J_c^{intra}\exp(-\theta_{GB}/\theta_0)$ in low field regime, the characteristic angle (θ_0) is estimated to around 7.9° for our Co-doped Ba-122 bicrystal films (fig.2 (c)), which is almost twice as large as that of $YBa_2Cu_3O_7$ [7].

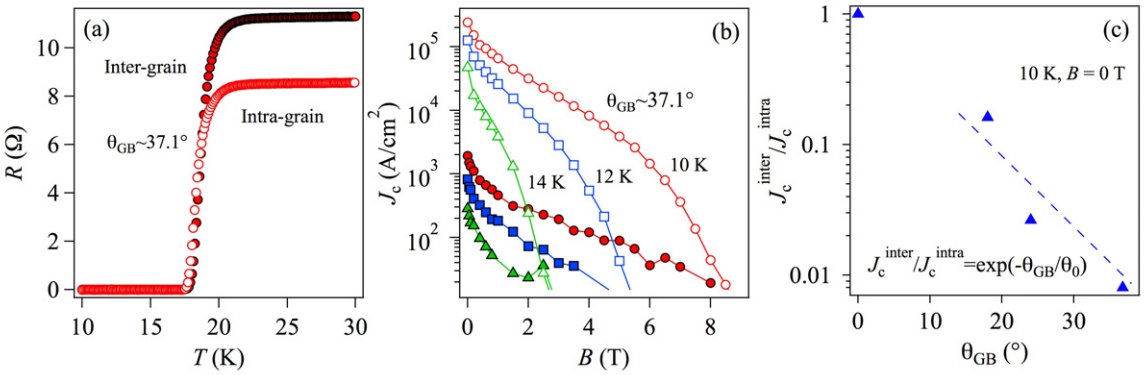

Fig. 2. (a) *R-T* curves of inter- and intra-grains. Both curves show the same T_c of around 20 K. (b) J_c-*B* performances ($B||c$) of the corresponding grains at different temperatures. Open symbols represent the intra-grain and the solid symbols show the inter-grain curves. (c) Normalized critical current density (J_c^{inter}/J_c^{intra}) as a function of θ_{GB} at 10 K.

The growth of epitaxial Fe with smooth surface on $SrTiO_3$ substrate is not straightforward, which is presumably due to the difference in crystal structure rather than to the lattice mismatch. As a result, epitaxial growth of Ba-122 is hardly achieved on Fe-buffered $SrTiO_3$. Indeed, fiber textured Fe is observed (fig. 3 (a)), when it is prepared directly on $SrTiO_3$ substrate with the same procedure as on MgO substrates. In order to avoid this problem, an additional buffer layer of $MgAl_2O_4$ between Fe and $SrTiO_3$ substrate has been used. $MgAl_2O_4$ fits better to accommodate the lattice mismatch to Fe rather than MgO as shown in Table 1. Here, the lattice mismatch is defined as $(a_f-a_s)/a_f$, where a_f and a_s are the lattice parameters of Fe and substrates, respectively. Additionally, a small lattice mismatch of 3.4 % between $MgAl_2O_4$ and $SrTiO_3$ may lead to good epitaxial growth of the $MgAl_2O_4$ buffer.

Fig. 3 (b) shows the 110 pole figure of Fe on $MgAl_2O_4$-buffered $SrTiO_3$ fabricated by the same procedure described in sub-section *2.1*. It is clear from fig. 3 (b) that a perfect textured growth of Fe is realized (average $\Delta\phi_{Fe}=0.61°$). During heating of Fe, evolution of the Fe-layer texture was observed through reflection high energy electron diffraction (RHEED), which is a similar observation of Fe on single crystalline MgO substrates.[8] The RHEED images of the Fe layer on $MgAl_2O_4$-buffered $SrTiO_3$ after the high temperature annealing showed only streak patterns, indicative of surface smoothing. This architecture also prevents the current-shunting effect between $SrTiO_3$ and Co-doped Ba-122. This buffer architecture offers the opportunity to grow smooth epitaxial Fe layers on various perovskite substrate such as (La,Sr)(Al,Ta)O_3(100) substrate (not shown in this paper).

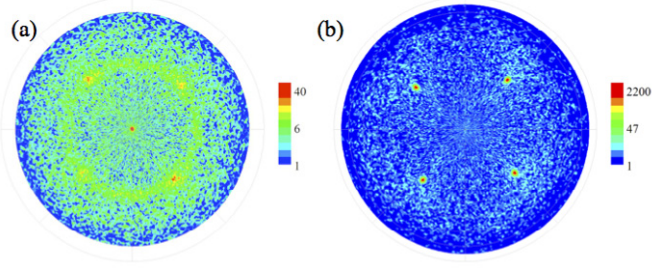

Fig. 3. (a) The 110 pole figure measurement of Fe on bare $SrTiO_3$ and (b) $MgAl_2O_4$-buffered $SrTiO_3$.

Table 1. The crystal structure, lattice parameter and the lattice mismatch to Fe of MgO and $MgAl_2O_4$.

Materials	Crystal structure	Lattice parameter (nm)	Lattice mismatch (%)
MgO	Rock salt	0.421	3.7
$MgAl_2O_4$	Spinel	0.8083 (a/2=0.4042)	-0.4

Structural characterization of Ba-122/Fe/$MgAl_2O_4$ on [001]-tilt GB $SrTiO_3$ substrate by means of X-ray diffraction is summarized in figs. 4. As stated earlier, *in-situ* Au layer deposition was conducted after the Ba-122 deposition, which explains the 111 reflection of Au in fig. 4 (a). It is further clear from fig. 4 (a) that only 00*l* reflections of Ba-122 with a small amount of the 110 reflection are observed. Fig. 4 (b) displays the ϕ-scans of the 103 Ba-122, the 110 Fe and the 110 $SrTiO_3$. Clear 8 peaks from two grains with a rotational angle of 30° are apparent. Accordingly, an epitaxial Ba-122 film is formed on [001]-tilt $SrTiO_3$ bicrystal substrate. The onset T_c = 24 K of the film is almost identical to that of Ba-122/Fe bilayers on single crystal substrates. (fig. 4 (c)) This value is higher than the intra-grain T_c deposited on MgO bicrystal presented in fig. 2 (a) due to a higher deposition temperature as well as different PLD targets (i.e. different Co concentration). The resultant bicrystal junctions show clear Josephson effects and the detailed studies can be found in Ref. [9].

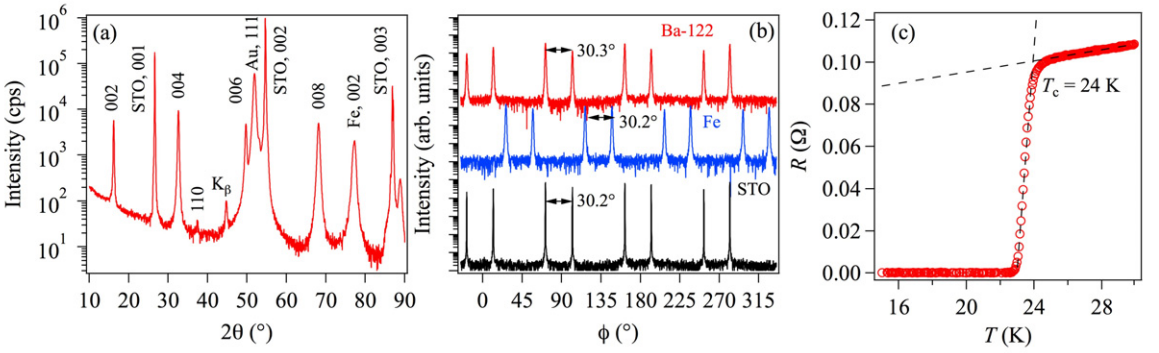

Fig. 4. (a) The θ/2θ scan of Ba-122/Fe/$MgAl_2O_4$ trilayer on [001]-tilt $SrTiO_3$ (STO) bicrystal substrate in Bragg- Brentano geometry using Co-Kα radiation. (b) The ϕ-scans of the 103 Ba-122, the 110 Fe, and 110 STO. Average misorientation angles are 30.3°, 30.2°, and 30.2° for Ba-122, Fe and STO, respectively. (c) Intra-grain T_c was recorded as 24 K.

4. Summary

High-quality Co-doped Ba-122 bicrystal films can be realized on both [001]-tilt MgO and $SrTiO_3$ substrates by employing Fe buffer layers via pulsed laser deposition. The additional $MgAl_2O_4$ buffer between Fe and $SrTiO_3$ is necessary for realizing epitaxial Ba-122. The characteristic angle of Co-doped Ba-122 in low field regime is about 8°, which is almost twice as large as that of $YBa_2Cu_3O_7$.

Acknowledgements

The authors would like to thank R. Hühne for fruitful discussions, K. Kühnel, and U. Besold for their technical support. This work was supported by DFG under Project Nos. BE 1749/13 and HA 5934/3-1. The research leading to these results has furthermore received funding from European Union's Seventh Framework Programme (FP7/2007-2013) under grant agreement number 283141 (IRON-SEA).

References

[1] Y. Kamihara, T. Watanabe, M. Hirano, H. Hosono, J. Am. Chem. Soc. 130 (2008) 3296.
[2] S. Lee, J. Jiang, J.D. Weiss, C.M. Folkman, C.W. Bark, C. Tarantini *et al.*, Appl. Phys. Lett. 95 (2009) 212505.
[3] T. Katase, Y. Ishimaru, A. Tsukamoto, H. Hiramatsu, T. Kamiya, K. Tanabe, H. Hosono, Nat. Commun. 2 (2011) 409.
[4] T. Thersleff, K. Iida, S. Haindl, M. Kidszun, D. Pohl, A. Hartmann *et al.*, Appl. Phys. Lett. 97 (2010) 022506.
[5] S. Trommler, R. Hühne, J. Hänisch, E. Reich, K. Iida, S. Haindl *et al.*, Appl. Phys. Lett. 100 (2012) 122602.
[6] K. Iida, S. Haindl, T. Thersleff, J. Hänisch, F. Kurth, M. Kidszun *et al.*, Appl. Phys. Lett. 97 (2010) 172507.
[7] H. Hilgenkamp, J. Mannhart, Rev. Mod. Phys. 74 (2002) 485.
[8] K. Iida, J Hänisch, S. Trommler, S. Haindl, F. Kurth, R. Hühne *et al.*, Supercond. Sci. Technol. 24 (2011) 125009.
[9] S. Schmidt, S. Döring, F. Schmidl, V. Tympel, S. Haindl, K. Iida *et al.*, IEEE Trans. Appl. Supercond. 23 (2013) 7300104.